Neuron
Article

RIM Determines Ca^{2+} Channel Density and Vesicle Docking at the Presynaptic Active Zone

Yunyun Han,[1] Pascal S. Kaeser,[2] Thomas C. Südhof,[2] and Ralf Schneggenburger[1,*]
[1]Laboratory of Synaptic Mechanisms, Brain Mind Institute, École Polytechnique Fédérale de Lausanne (EPFL), 1015 Lausanne, Switzerland
[2]Department of Molecular and Cellular Physiology and Howard Hughes Medical Institute, Stanford University School of Medicine, Lorry Lokey Stem Cell Research Building, 265 Campus Drive, Stanford, CA 94305-5453, USA
*Correspondence: ralf.schneggenburger@epfl.ch
DOI 10.1016/j.neuron.2010.12.014

SUMMARY

At presynaptic active zones, neurotransmitter release is initiated by the opening of voltage-gated Ca^{2+} channels close to docked vesicles. The mechanisms that enrich Ca^{2+} channels at active zones are, however, largely unknown, possibly because of the limited presynaptic accessibility of most synapses. Here, we have established a Cre-lox based conditional knockout approach at a presynaptically accessible central nervous system synapse, the calyx of Held, to directly study the functions of RIM proteins. Removal of all RIM1/2 isoforms strongly reduced the presynaptic Ca^{2+} channel density, revealing a role of RIM proteins in Ca^{2+} channel targeting. Removal of RIMs also reduced the readily releasable pool, paralleled by a similar reduction of the number of docked vesicles, and the Ca^{2+} channel-vesicle coupling was decreased. Thus, RIM proteins co-ordinately regulate key functions for fast transmitter release, enabling a high presynaptic Ca^{2+} channel density and vesicle docking at the active zone.

INTRODUCTION

Action potentials (APs) evoke neurotransmitter release from presynaptic nerve terminals in the process of SNARE-protein-mediated vesicle fusion (Chen and Scheller, 2001; Jahn et al., 2003). Transmitter release is triggered by Ca^{2+} influx through voltage-gated Ca^{2+} channels, and the fast phase of release closely follows the waveform of presynaptic Ca^{2+} current with only a submillisecond delay (Sabatini and Regehr, 1996; Borst and Sakmann, 1996). One prerequisite for the temporal precision of transmitter release is a tight spatial colocalization between docked vesicles and Ca^{2+} channels in the range of a few 10 s of nanometers, which enables a short diffusional distance between Ca^{2+} channels and the Ca^{2+} sensor for vesicle fusion (see Neher, 1998 for a review). Thus, there is general agreement that Ca^{2+} channels must be enriched within the active zone, as is also suggested from fast Ca^{2+} imaging studies (Llinás et al., 1995; Zenisek et al., 2003) and from initial ultrastructural evidence at central nervous system (CNS) synapses (Bucurenciu et al., 2008). However, the molecular mechanisms that enable an enrichment of Ca^{2+} channels at the presynaptic active zone are not well understood.

The presynaptic active zone of synapses consists of a dense accumulation of cytomatrix proteins, some of which, like Munc13, ELKS/CAST, and RIMs, are localized highly specifically at active zones (Schoch and Gundelfinger, 2006). Among these, RIM proteins (Rab3-interacting molecules; Wang et al., 1997) are interesting candidates for scaffolding proteins with possible interactions with voltage-gated Ca^{2+} channels (Coppola et al., 2001; Hibino et al., 2002; Kiyonaka et al., 2007). RIM proteins are encoded by four genes (*Rims1–4*) that drive the expression of seven known RIM isoforms: RIM1α, 1β and RIM2α, 2β, and 2γ, as well as RIM3γ and RIM4γ (Wang et al., 2000; Wang and Südhof, 2003; Kaeser et al., 2008). RIM proteins bind to multiple other presynaptic proteins—e.g., Rab3, Munc13's, α-liprins, and RIM-binding proteins (RIM-BPs; Wang et al., 1997, 2000; Betz et al., 2001; Schoch et al., 2002; Dulubova et al., 2005). Genetic removal of RIM1α in mice and of the homologous unc10 protein in *Caenorhabditis elegans* has indicated a role of RIMs in transmitter release (Koushika et al., 2001; Schoch et al., 2002; Calakos et al., 2004) as well as in presynaptic forms of long-term plasticity in a synapse-specific way (Castillo et al., 2002). Recent studies proposed multiple potential interactions between RIMs and Ca^{2+} channels. RIM C2 domains were found to bind to L- and P/Q-type Ca^{2+}channels (Coppola et al., 2001). Heterologous expression of RIM1α in nonneuronal cells reduced the inactivation of coexpressed voltage-gated Ca^{2+} channels via an interaction of the RIM1 C terminus with Ca^{2+} channel β4 subunits (Kiyonaka et al., 2007). RIM-BPs have been found to bind to L- and N-type Ca^{2+} channel α subunits (Hibino et al., 2002). However, the role of RIM proteins for Ca^{2+} entry at the presynaptic nerve terminal has remained unclear, maybe because no previous study eliminated all RIM1/2 isoforms in vertebrates. Another reason is that genetically accessible model synapses, like the neuromuscular junctions of *C. elegans* and *Drosophila* and cultured CNS neurons, are not accessible to direct presynaptic recordings.

The calyx of Held in the auditory brainstem is a large synapse accessible to patch-clamp recordings directly at the nerve terminal, which has enabled a uniquely direct control of presynaptic Ca^{2+} for studying the Ca^{2+} regulation of transmitter release (see Schneggenburger and Forsythe, 2006 for a review). However, the usefulness of the calyx preparation has been limited by the fact that many conventional mouse knock out (KO) models are perinatally lethal. To overcome this limitation

and to allow for a direct study of the presynaptic roles of RIM proteins, we have devised a Cre-lox based conditional KO approach at the calyx of Held synapse, using recently generated RIM1/2 floxed mouse lines (Kaeser et al., 2011). We show that the conditional removal of RIM proteins leads to a strong decrease of Ca^{2+} currents in the nerve terminal, providing direct evidence that RIMs enrich Ca^{2+} channels at the presynaptic active zone. RIM1/2 removal also led to a marked reduction in the number of readily releasable vesicles, which was paralleled by a similar reduction in the number of docked vesicles. Moreover, RIM proteins help to speed the rates of transmitter release both intrinsically and by increasing the coupling of readily releasable vesicles with Ca^{2+} channels. Thus, RIM proteins coordinate essential functions that ensure fast rates of transmitter release at synapses.

RESULTS

Conditional Knock Out of RIM1/2 at the Calyx of Held Synapse

We wished to investigate the presynaptic function of RIM proteins at the calyx of Held, a large CNS model synapse at which direct measurement of presynaptic Ca^{2+} currents can be made (see Introduction). However, constitutive RIM1α/RIM2α double KO mice die at birth (Schoch et al., 2006), which precludes their analysis at the calyx of Held, and deleting individual RIM isoforms might produce only a weak phenotype because of the functional redundancy among the isoforms (Schoch et al., 2006; Kaeser et al., 2008). We therefore aimed to remove RIM1/2 conditionally at the calyx of Held, using recently produced floxed mouse lines in which the expression of all RIM1 and RIM2 isoforms, including RIM1β and RIM2β, can be abolished by expression of Cre-recombinase (Kaeser et al., 2011). For this purpose, we searched for a Cre-driver mouse line that expresses Cre-recombinase specifically in the lower auditory brainstem where calyces of Held are located. We found that in Krox20+/Cre mice (Voiculescu et al., 2000), Cre-activity as revealed by a tandem-dimer red fluorescence protein (tdRFP) reporter mouse line (Luche et al., 2007) was present in the lower auditory brainstem as well as in the trigeminal nucleus and some adjacent areas, but importantly, most other areas of the brainstem and CNS were devoid of Cre activity (Figure S1A, available online). In the ventral cochlear nucleus, which harbors globular bushy cells that generate calyces of Held (see Cant and Benson, 2003, and references therein), a large number of tdRFP-positive neurons were found (Figure S1B and Figure 1A). In the medial nucleus of the trapezoid body (MNTB), the target nucleus of calyces of Held, tdRFP was present in postsynaptic neurons, as well as in calyces of Held, which were identified by costaining with an anti-synaptotagmin2 (Syt2) antibody (Figure 1B). Thus, Cre activity in Krox20+/Cre mice is present in a neuron population that includes calyx of Held-generating neurons in the cochlear nucleus, which explains the presence of tdRFP-positive large nerve endings in the MNTB.

We crossed the Krox20Cre/+ mice with floxed RIM1/2 mice (Kaeser et al., 2011) to generate conditional RIM1/2 double KO mice specific for the auditory brainstem. Because of germline recombination in the Krox20Cre line (Voiculescu et al., 2000), we obtained Cre-positive RIM1/2 lox/Δ mice (see Experimental Procedures). These mice were viable and fertile, which allowed us to investigate synaptic transmission in brain slice preparations. We will refer to synapses recorded in Cre-positive RIM1/2 lox/Δ mice as RIM1/2 cDKO synapses (for conditional double KO). As a control group, we used Cre-negative, RIM1/2 lox/Δ littermate mice (see Experimental Procedures). Excitatory postsynaptic currents (EPSCs) evoked by afferent fiber stimulation at calyx of Held synapses in RIM1/2 cDKO mice had amplitudes of only 1.86 ± 1.73 nA (n = 12 cells), significantly smaller than in Cre-negative littermate control mice (9.8 ± 4.2 nA; n = 15 cells; Figures 1C and 1D). The evoked EPSCs also had slightly, but significantly slower rise times (Figures 1E and 1F; p = 0.0038), reflecting slowed release kinetics that will be analyzed in more detail below (see Figures 4 and 5). The amplitude of spontaneous, miniature EPSCs (mEPSCs) was unchanged (Figure 1G), consistent with a presynaptic transmitter release deficit. Synaptic phenotypes were consistently observed in all synapses studied in RIM1/2 cDKO mice (n = 73). This indicates that Cre-mediated removal of the RIM proteins was effective, without detectable inhomogeneity across the population of the studied neurons.

RIMs Determine Presynaptic Ca^{2+} Channel Density

Having established the conditional removal of all long RIM isoforms at the calyx of Held, we are now in a position to directly study the presynaptic function of RIM1/2 proteins. In current clamp recordings from calyces of Held, presynaptic APs elicited by afferent fiber stimulation were unchanged in RIM1/2 cDKO calyces (Figure 2), showing that changes in the AP waveform do not underlie the reduced transmitter release. We next investigated presynaptic Ca^{2+} currents in voltage-clamp recordings of the calyx of Held. Surprisingly, these recordings revealed a strong reduction of the amplitude of Ca^{2+} currents in RIM1/2 cDKO calyces (Figure 2C). In both genotypes, presynaptic Ca^{2+} currents started to activate at around −20 mV and the maximal Ca^{2+} current was observed at ~0 mV (Figures 2C and 2D); however, the maximal Ca^{2+} current was only 500 ± 310 pA (n = 19 cells) in RIM1/2 cDKO calyces, whereas it was 1040 ± 250 pA (n = 9) in calyces of control mice (Figure 2E; $p < 0.001$). Control experiments with Krox20+/Cre mice and with RIM1lox/RIM2lox mice revealed no significant reduction of the presynaptic Ca^{2+} current (Figure S2), showing that the reduced Ca^{2+} currents were not caused by the Krox20+/Cre allele nor by the nonrecombined, floxed RIM1/2 alleles. In order to normalize the measured Ca^{2+} current amplitudes for the membrane surface of calyx terminals, we recorded the membrane capacitance C_m of calyces of Held, which was unchanged (12.7 ± 4.0 pF, n = 19 and 14.8 ± 3.5 pF, n = 9 in RIM1/2 cDKO and control calyces, respectively; p = 0.16). The maximal Ca^{2+} current normalized for membrane surface (peak I_{Ca} / C_m) was significantly smaller in RIM1/2 cDKO calyces as compared to control mice (Figure 2F, $p < 0.001$).

Since RIM1α expression was shown to reduce voltage-dependent inactivation of Ca^{2+} channels in BHK cells (Kiyonaka et al., 2007), we next tested whether the reduced Ca^{2+} current amplitude might result from an increased steady-state inactivation at the standardly employed holding potential of −70 mV.

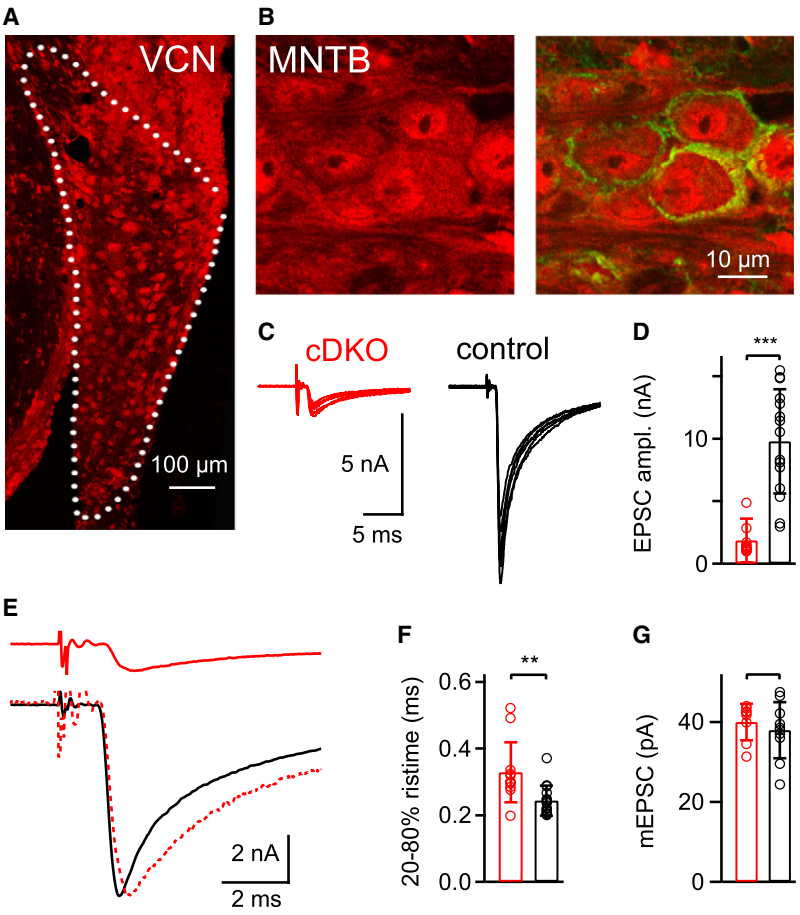

Figure 1. Conditional Removal of RIM1/2 in the Auditory Brainstem Leads to Strong Reduction of Transmitter Release at the Calyx of Held

(A and B) Krox20-driven Cre activity in the VCN (A) and MNTB (B) as revealed by anti-RFP immunohistochemistry with a td-RFP reporter mouse (red channel). In (A), Cre activity was observed in many VCN neurons, most likely including globular bushy cells that give rise to calyces of Held. Correspondingly, in (B) immunohistochemistry against RFP and against the presynaptic marker synaptotagmin-2 (green channel; right) shows the presence of RFP in presynaptic calyces of Held as well as in MNTB principal cells.

(C) Fiber stimulation-evoked EPSCs at the calyx of Held synapse of a Cre-positive, RIM1lox/Δ, RIM2lox/Δ mouse (referred to as "cDKO", left), and in a Cre-negative control mouse (right). n = 6 consecutive traces are shown for individual cells.

(D) Average and individual values of evoked EPSC amplitudes in RIM1/2 cDKO synapses (n = 12 cells) and in control synapses (n = 15 cells).

(E) Average EPSC traces of the same cells as shown in (C). Lower: An overlay of the EPSC from a control mouse and a peak-scaled EPSC from a RIM1/2 cDKO mouse illustrate a slight slowing of the EPSC rise time in the RIM1/2 cDKO mice.

(F) Average and individual values of the 20%–80% rise times. There was a small but significant ($p = 0.0038$) slowing in RIM1/2 cDKO mice.

(G) Average and individual values of mEPSC amplitudes in the two genotypes; there was no statistically significant difference ($p > 0.05$). In this and all subsequent figures red and black symbols refer to data from RIM1/2 cDKO synapses and control synapses respectively. Star symbols indicate statistical significance (*$p < 0.05$; **$p < 0.01$; and ***$p < 0.001$) and a bracket without star symbol indicates no statistical significance ($p > 0.05$; Student's t test). The error bars represent SD. See also Figure S1.

Conditioning prepulses of 2 s duration to more hyperpolarized membrane potentials (−90 mV, −110 mV; Figures 2G and 2H) did not significantly increase the Ca^{2+} current during a subsequent step to 0 mV, arguing against significant steady-state inactivation at the holding potential. Therefore, the reduced Ca^{2+} current amplitude most likely reflects a reduced number of Ca^{2+} channels in the calyx of Held nerve terminals. With conditioning prepulses to more positive membrane potentials (−50 and −30 mV), we found a somewhat stronger steady-state inactivation in RIM1/2 cDKO calyces as compared to control (Figure 2H; $p < 0.01$), consistent with previous work in cultured nonneuronal cells (Kiyonaka et al., 2007). Overall, however, our data failed to show a strong effect of RIM1/2 removal on the inactivation of presynaptic Ca^{2+} currents, at least for short depolarizing steps of up to 20 ms lengths (Figure 2C).

In wild-type calyces of Held, about 80% of the presynaptic Ca^{2+} current is mediated by P/Q-type Ca^{2+} channels and N- and R-type Ca^{2+} channels make up the rest (Wu et al., 1999; Iwasaki et al., 2000). To test whether the reduction of the presynaptic Ca^{2+} current is accompanied by a change in the contribution of Ca^{2+} channel subtypes, we blocked Ca^{2+} currents sequentially with the P/Q-type-specific toxin ω-agatoxin-IVa (agatoxin; 0.2 µM; Figure 2I, green traces) followed by the N-type-specific toxin ω-conotoxin-GVIa (conotoxin; 3 µM) in the continued presence of agatoxin (Figure 2I; blue traces). In RIM1/2 cDKO calyces, 80.6% ± 14% of the Ca^{2+} current was blocked by agatoxin, similar to the value in control calyces (92% ± 7.1%; $p = 0.14$; Figure 2J). Another 14.7% ± 10.3% of the initial Ca^{2+} current in RIM1/2 cDKO calyces was blocked by conotoxin, as compared to 8.2% ± 7.2% in control calyces. Thus, removal of RIM1/2 does not significantly alter the relative contribution of P/Q- and N-type Ca^{2+} channels. Taken together, direct recordings from the nerve terminal reveal a strong reduction of presynaptic Ca^{2+} currents in RIM1/2 cDKO neurons, which is specific for the nerve terminal since Ca^{2+} currents in the soma/dendritic compartment of MNTB neurons were unchanged (Figure S2). Thus, RIM proteins have a so far unrecognized role in enriching voltage-gated Ca^{2+} channels at the presynaptic nerve terminal (see also Kaeser et al., 2011).

RIMs Ensure a Large Readily Releasable Pool and Influence Release Probability

We showed that conditional removal of RIM1/2 leads to a strong reduction of transmitter release (by ~80%; Figure 1) and that presynaptic Ca^{2+} currents are strongly reduced (~50%; Figure 2). Does the reduced transmitter release primarily reflect

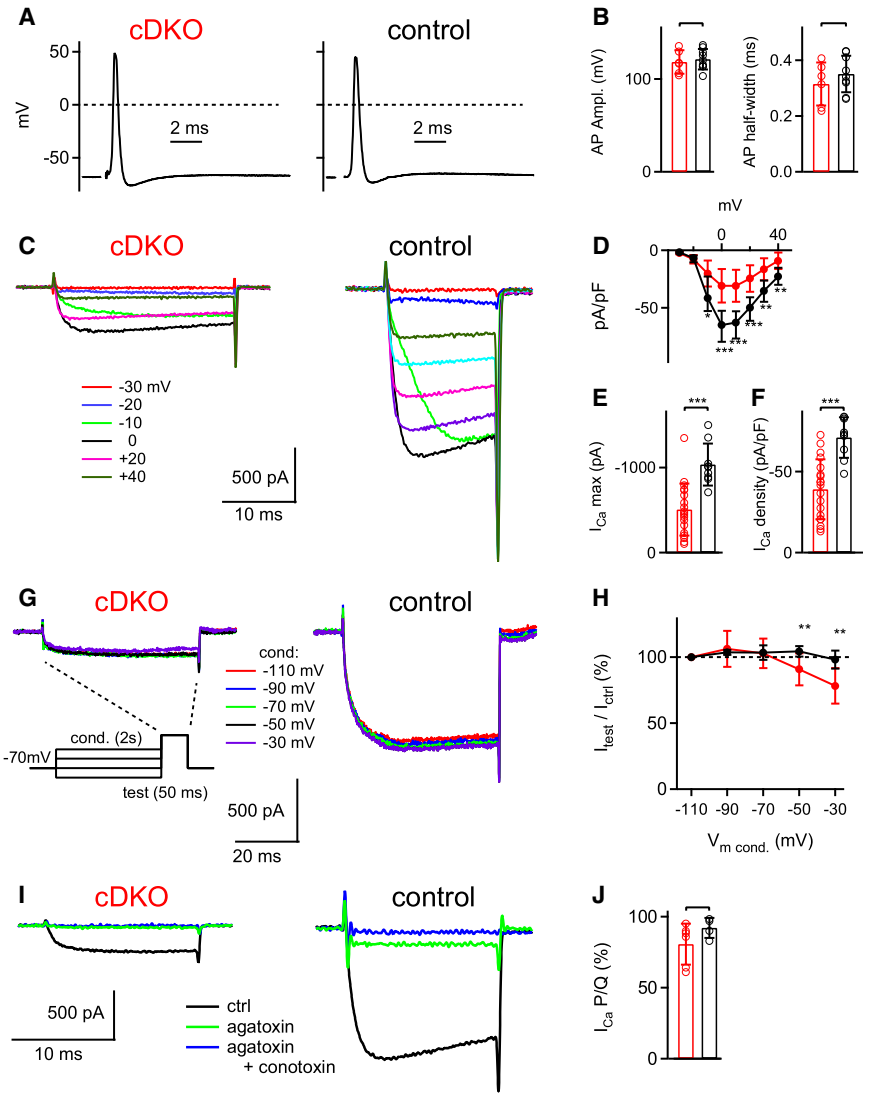

Figure 2. A Strong Reduction of Ca^{2+} Current Density in Nerve Terminals of RIM1/2 cDKO Mice

(A and B) Presynaptic action potentials (APs) recorded in RIM1/2 cDKO calyces (A, left), and in control calyces (A, right) following afferent fiber stimulation. The average AP amplitudes and AP-halfwidths were unchanged in RIM1/2 cDKO calyces (B).

(C) Ca^{2+} currents evoked by voltage steps to the indicated membrane potentials in a RIM1/2 cDKO calyx (left) and in a control calyx (right).

(D) Current voltage relationship of Ca^{2+} currents normalized by presynaptic membrane capacitance (C_m), averaged for n = 19 RIM1/2 cDKO calyces and for n = 9 control calyces.

(E and F) Peak Ca^{2+} current amplitude (E) and Ca^{2+} current density (F) following normalization by the presynaptic C_m in RIM1/2 cDKO calyces (red) and in control calyces (black).

(G and H) Presynaptic Ca^{2+} currents in response to a 50 ms test pulse to 0 mV, recorded after conditioning prepulses of 2 s duration to the indicated membrane potentials. Note that negative prepulses did not reveal any significant steady-state inactivation at −70 mV, the holding potential standardly used here. In (H), the percentage of the current measured during the test pulse, relative to the current obtained for the most negative conditioning pulse, is given.

(I and J) Sequential block of presynaptic Ca^{2+} currents by ω-agatoxin-IVa (agatoxin, 0.2 μM; green trace), and by the subsequent application of ω-conotoxinGVIa (conotoxin, 3 μM) in the continuous presence of agatoxin (blue traces). The fraction of the total Ca^{2+} current blocked by agatoxin in the two genotypes was unchanged (J).

The error bars represent SD. See also Figure S2.

a reduced release probability caused by the much smaller presynaptic Ca^{2+} influx or are there other factors, like a reduced readily releasable pool of vesicles (Calakos et al., 2004), which contribute to the decreased transmitter release? To investigate changes in pool size and release probability, we next used brief high-frequency trains of afferent fiber stimulation to measure the size of the readily releasable pool (Figure 3; Schneggenburger et al., 1999). In control synapses, the first EPSC was large (~8 nA in Figure 3A), and subsequent EPSCs decreased in amplitude to a new steady-state value (Figures 3A and 3B, right). In contrast, RIM1/2 cDKO synapses had much smaller EPSCs (~2 nA in Figure 3A), and depression usually only occurred after the third or fourth stimulus (Figures 3A and 3B, left; see also Figure 3D for the average of all cells). To quantify the onset of depression, we made line fits to relative depression curves in the range of the first to the sixth stimulus (Figure 3B, blue fit lines). This analysis gave slopes of −62% ± 26% per five stimuli (n = 8) and −27% ± 33% per five stimuli (n = 9) for control and RIM1/2 cDKO synapses, respectively ($p < 0.05$; see also Figure 3D, bottom, for line fits to the averaged data sets for each genotype). Thus, the onset of depression was significantly slowed in RIM1/2 cDKO synapses, which suggests a decreased release probability of any given readily releasable vesicle.

We next analyzed the apparent size of the readily releasable pool by using the method of cumulative EPSC amplitudes back-extrapolated to time zero (Schneggenburger et al., 1999; Figure 3C). The back-extrapolated cumulative EPSC amplitude was 51.1 ± 16.2 nA in control mice (corresponding to ~1700 vesicles, assuming an average mEPSC amplitude of 30 pA; n = 8 cells), but only 11.9 ± 6.9 nA in RIM1/2 cDKO mice (~400 vesicles; n = 10 cells). Thus, there was a clear pool size reduction in RIM1/2 cDKO synapses ($p < 0.001$; Figure 3E). The average release probability, calculated by dividing the first EPSC amplitude by the pool size estimate (Iwasaki and Takahashi, 2001) was 0.27 ± 0.09 (n = 8) and 0.19 ± 0.05 (n = 9) in control and RIM1/2 cDKO synapses, respectively ($p = 0.04$; Figure 3F).

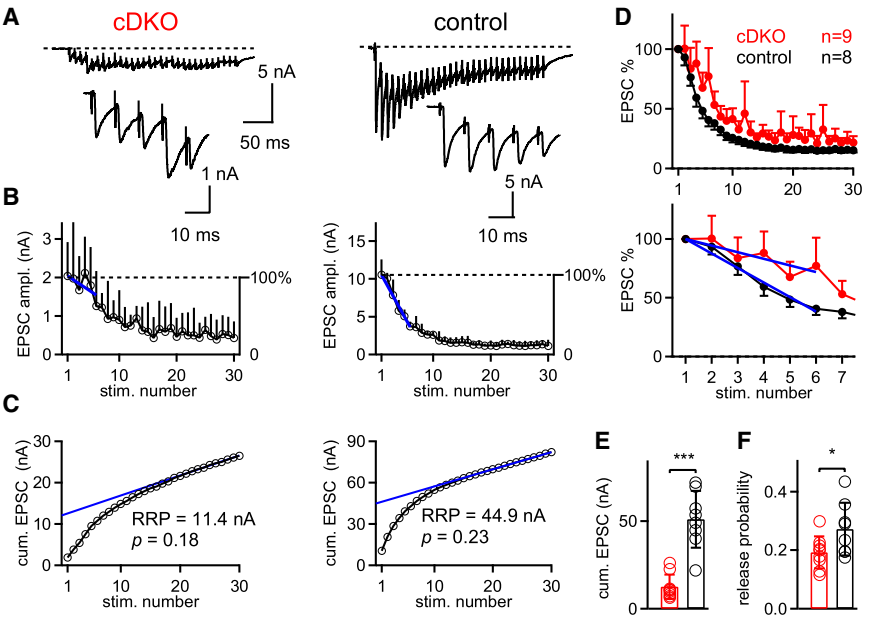

Figure 3. Train Stimulation and Short Term Plasticity Experiments Indicate a Reduced Pool Size and a Slightly Lowered Release Probability

(A) Example single EPSC traces in response to 100 Hz trains of afferent fiber stimulations in a RIM1/2 cDKO synapse (left) and in a control synapse (right). The first five EPSCs during the train are shown on increased scales in the insets.

(B) EPSC depression curves averaged over six and seven trials for the same cells as shown in (A). The first six data points following normalization to the first EPSC amplitude (see right *y* axis) were fitted with linear functions to quantify the onset of depression in both genotypes (blue fit lines).

(C) Cumulative EPSC amplitude plots for the two cells shown in (A and B). Back-extrapolation to time zero yields the recovery-corrected pool size estimate (Schneggenburger et al., 1999). Note the much smaller value in the RIM1/2 cDKO neuron (left) as compared to the control cell (right). Data in A–C are from corresponding recordings.

(D) Plot of the normalized EPSC amplitudes during 100 Hz trains, averaged for all RIM1/2 cDKO (n = 9 cells) and control cells (n = 8). Lower: The data on an expanded time scale together with the line fits to the average data set (blue lines). The error bars represent SEM.

(E and F) Individual and average values of the pool size estimate (E) and of the release probability (F) for RIM1/2 cDKO (red) and control synapses (black). The error bars represent SD in (B, E, and F) and SEM in (D).

These experiments with high-frequency trains show that the release deficit is primarily caused by a decreased pool of readily releasable vesicles (reduction by ~75%; Figure 3E). In addition, there was also a small but significant reduction of the release probability (by ~25%), which might explain the observed slowing in the onset of synaptic depression.

Ca^{2+} Uncaging Reveals a Smaller Fast Releasable Pool and a Decreased Ca^{2+} Sensitivity of Release

We showed that in the absence of RIM1/2, the number of presynaptic Ca^{2+} channels was reduced by ~50% (Figure 2) and the readily releasable pool was strongly reduced, together with a small reduction of the release probability (Figure 3). To study the reduced readily releasable pool size more directly, we used Ca^{2+} uncaging to strongly stimulate release independent of Ca^{2+} channel opening. In addition, Ca^{2+} uncaging will allow us to address the possibility of a reduced intrinsic Ca^{2+} sensitivity of release in RIM1/2 cDKO synapses, which could underlie the reduced release probability.

In RIM1/2 cDKO synapses, Ca^{2+} uncaging stimuli evoked EPSCs with small amplitudes (~6 nA in the example of Figure 4B, left) and flashes that elevated $[Ca^{2+}]_i$ above ~15 μM did not evoke EPSCs with larger amplitudes in RIM1/2 cDKO synapses (Figure 4B), showing directly the limited pool of readily releasable vesicles in RIM1/2 cDKO synapses. The maximal EPSC amplitudes at 10–15 μM $[Ca^{2+}]_i$ were much smaller in RIM1/2 cDKO synapses (5.7 ± 4.9 nA, n = 7) than in control synapses (14.2 ± 7.8 nA, n = 6; $p < 0.01$), indicating a reduced pool size. To analyze the number of releasable vesicles and their release kinetics in more detail, we deconvolved the Ca^{2+} uncaging-evoked EPSCs to reveal rates of transmitter release (Figure 4B, inset) and cumulative release rates (Figure 4C). These were best fitted by the sum of at least two exponential functions (see Experimental Procedures), indicating a fast and a slow release component in response to Ca^{2+} uncaging (Wölfel et al., 2007; Kochubey et al., 2009). Thus, the pool of readily releasable vesicles can be kinetically subdivided into a fast releasable pool (FRP) and a slowly releasable pool (SRP) (Sakaba and Neher, 2001; Wölfel et al., 2007). To estimate the size of the FRP, we analyzed the number of vesicles released in the fast release component in response to $[Ca^{2+}]_i$ steps to 10–15 μM. The FRP was strongly reduced, from 1091 ± 396 vesicles in control synapses to 271 ± 178 vesicles in RIM1/2 cDKO synapses (n = 6 and 7 respectively; Figure 4D). In addition, the amplitude of the slow-release component was also reduced, from 833 ± 658 to 211 ± 205 vesicles in control and RIM1/2 cDKO synapses, respectively ($p = 0.036$).

We next plotted the absolute peak release rates as a function of the presynaptic $[Ca^{2+}]_i$ step amplitude (Figure 4E). This plot showed that the peak release rates were significantly smaller at all $[Ca^{2+}]_i$ in RIM1/2 cDKO synapses as compared to control ($p < 0.001$; analysis of covariance, ANCOVA). However, the absolute peak release rates at any given $[Ca^{2+}]_i$ are a function of the intrinsic Ca^{2+} sensitivity of release, as well as of the absolute pool size. To normalize for the reduced FRP size in the RIM1/2 cDKO synapses, we divided the absolute peak release rates by the FRP estimated in each cell pair. This revealed slightly reduced pool-normalized release rates in RIM1/2 cDKO synapses (Figure 4F), but this difference did not reach statistical significance ($p = 0.13$; ANCOVA). In contrast, other kinetic parameters of release, like the minimal delay and the fast release time constant, showed a significant slowing at all $[Ca^{2+}]_i$ investigated ($p < 0.001$ and $p < 0.01$; see Figures 4G and 4H), indicating

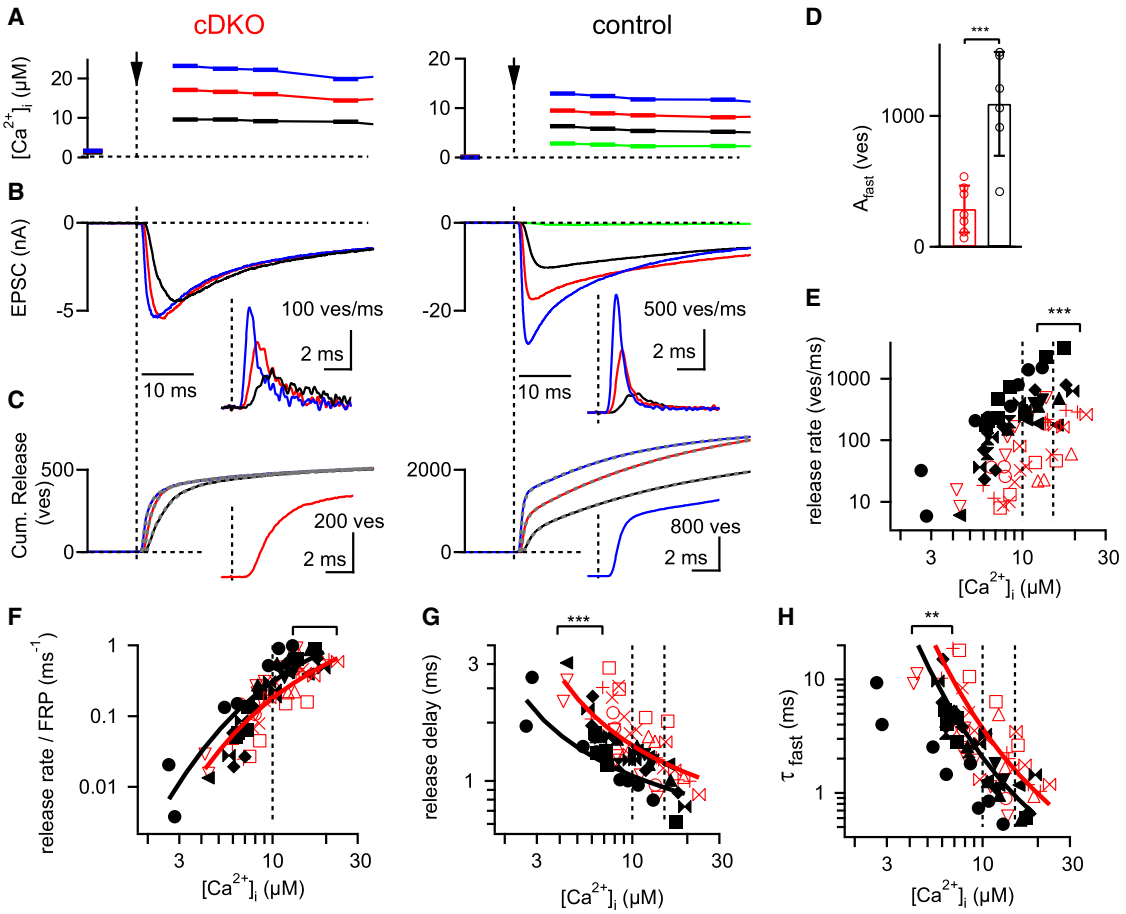

Figure 4. Presynaptic Ca^{2+} Uncaging Reveals a Smaller Readily Releasable Pool and a Decrease in the Intrinsic Ca^{2+} Sensitivity

(A–C) Ca^{2+} uncaging-evoked presynaptic $[Ca^{2+}]_i$ steps (A), postsynaptic EPSCs (B), and cumulative transmitter release (C) in a RIM1/2 cDKO (left) and control synapse (right). The insets in (B) show the transmitter release rates. Note the much smaller Ca^{2+} uncaging-evoked EPSCs in the RIM1/2 cDKO synapse, which indicate a strongly reduced readily releasable pool. The cumulative release traces in (C) were best fitted with double-exponential or double-exponential plus line functions (Dashed gray traces; see Experimental Procedures). The insets in (C) show cumulative release traces in response to roughly similar $[Ca^{2+}]_i$ steps (~15 μM) on an expanded time-scale, to illustrate the slowed rise and longer delay in RIM1/2 cDKO synapses.

(D) The number of fast-released vesicles for $[Ca^{2+}]_i$ steps in the range of 10–15 μM, as obtained by the amplitude parameter of the fast fit component of double-exponential fits to the cumulative release traces (see [C]).

(E) Plot of the peak transmitter release rates as a function of the $[Ca^{2+}]_i$ step amplitude for both genotypes. The statistical significance between the data sets was determined by ANCOVA ($p < 0.001$).

(F–H) Pool-normalized peak release rate (F), release delays (G), and the time constant of the fast release component (H) plotted against the amplitude of the $[Ca^{2+}]_i$ steps. Note the significantly slower release delays (G) ($p < 0.001$; ANCOVA) and fast release time constants (H) ($p < 0.01$; ANCOVA). The five-site model of Ca^{2+} binding and vesicle fusion (Schneggenburger and Neher, 2000) was globally fitted to all three data sets (F, G, and H) for each genotype. The resulting fit parameters indicate that slowed Ca^{2+} binding (decreased on rate, and slightly decreased off rate; see Experimental Procedures for parameters) could describe the data in the RIM1/2 cDKO synapses. The error bars represent SD.

that the intrinsic Ca^{2+} sensitivity of release was lower in the absence of RIM1/2.

To analyze the lowered intrinsic Ca^{2+} sensitivity quantitatively, the kinetic data, as well as the pool-normalized peak release rates, were globally fitted by a model of cooperative Ca^{2+} binding and vesicle fusion (Schneggenburger and Neher, 2000). The fits showed that a lowering of the on rate of Ca^{2+} binding (k_{on}) and a slight lowering of the off rate (k_{off}) led to a good description of the RIM1/2 cDKO data as compared to the control synapses (Figures 4F–4H; red and black fit lines, respectively; see Experimental Procedures for model parameters). The Ca^{2+} uncaging experiments, therefore, show that RIM1/2 proteins determine the size of the readily releasable pool since both the FRP and SRP were reduced, and RIM1/2 increases the intracellular Ca^{2+}-sensitivity of release by a factor of ~1.5- to 2-fold.

RIM Proteins Contribute to Ca^{2+} Channel-Vesicle Coupling

We have shown that RIM proteins are necessary to enrich Ca^{2+} channels at the presynaptic nerve terminal (Figure 2) and to maintain a high number of readily releasable vesicles (Figures 3and 4). How well are the remaining readily releasable vesicles

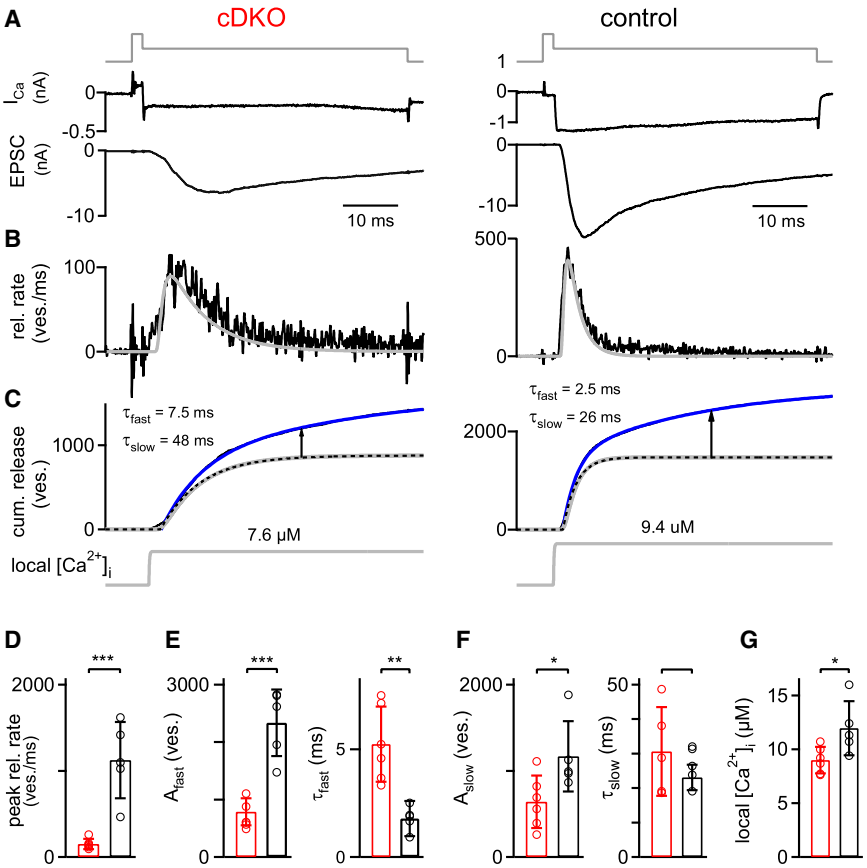

Figure 5. Paired Pre- and Postsynaptic Recordings Show a Deficit in Ca^{2+} Channel-Release Coupling in Addition to the Strongly Decreased Pool Size

(A–C) Transmitter release in response to prolonged presynaptic depolarizations. Ca^{2+} currents and EPSCs (A, upper and lower panel), release rates (B), traces of cumulative release (C, upper), and the back-calculated local $[Ca^{2+}]_i$ signal (C, lower) are shown. The double-exponential (best) fit of the cumulative release traces is overlaid as a blue line over the data (black lines, not visible). The dotted black traces in (C) are the fast components of the double-exponential fits. The gray traces overlaid over the transmitter release rates (B) and the fast release component (C) are the predicted release rates determined by the back-calculation approach with the five-site model of Ca^{2+} binding and vesicle fusion (Schneggenburger and Neher, 2000), which effectively models the fast release component. The arrows show the estimated amplitude of the slow release component at a time of 30 ms.

(D) Average peak release rates of both genotypes.

(E) Estimate of the FRP size obtained from the amplitude parameter of the fast release component (left, in number of vesicles) and time-constant of the fast release component (right) for both genotypes.

(F) Number of slowly released vesicles (left) and slow release time-constant (right) for both genotypes.

(G) Average and individual values of the amplitude of the back-calculated local $[Ca^{2+}]_i$ as shown in C (lower; gray traces). Note the slightly, but significantly ($p = 0.03$) smaller local $[Ca^{2+}]_i$ that was back-calculated for the RIM1/2 cDKO synapses. The error bars represent SD. See also Figure S3.

coupled to the remaining Ca^{2+} channels? To address this question, we made paired pre- and postsynaptic recordings and performed a kinetic analysis of transmitter release in response to Ca^{2+} influx through voltage-gated Ca^{2+} channels (Figure 5). Analyzing such data in the light of the intracellular Ca^{2+} sensitivities as determined by Ca^{2+} uncaging for each genotype (Figure 4) should then allow us to examine the efficiency of the coupling between Ca^{2+} channels and readily releasable vesicles (Wadel et al., 2007).

In most experiments, the presynaptic membrane potential was briefly stepped to +80 mV to open Ca^{2+} channels rapidly and then returned to 0 mV to admit a pulse-like presynaptic Ca^{2+} influx (Figures 5A and 5B, top; Sakaba and Neher, 2001). As expected, the resulting Ca^{2+} currents were smaller in RIM1/2 cDKO calyces (Figure 5A, top), and the EPSCs in response to such pool-depleting Ca^{2+} currents were significantly smaller in RIM1/2 cDKO synapses (6.8 ± 2.4 nA; n = 6) as compared to control (25.9 ± 6.4 nA; n = 5; $p < 0.001$), indicative of the reduced pool size (see above). Interestingly, the 20%–80% rise time of the EPSCs was prolonged in RIM1/2 cDKO synapses (3.4 ± 1.5 ms; n = 6) as compared to control synapses (1.24 ± 0.4 ms, n = 5; p = 0.012), which indicates an additional deficit in the kinetics of transmitter release.

To investigate the defects in release kinetics in more detail, we deconvolved the EPSCs to derive transmitter release rates (Figure 5B, black traces) and traces of cumulative release (Figure 5C, black trace below blue fit line). The peak release rates were strongly reduced in RIM1/2 cDKO synapses (Figure 5D) and the width of the transmitter release at half-maximal amplitudes was longer in RIM1/2 cDKO synapses (5.1 ± 1.8 ms, n = 6) than in control (2.3 ± 1.1 ms, n = 5; $p < 0.05$). The integrated release rate traces were fitted with a series of single- and double-exponential function with or without line component to determine the best fit function (see Experimental Procedures). In both genotypes, cumulative release was best fitted by functions that contained at least two exponential components (Figure 5C, blue fit lines), indicating a fast and a slow release component (Sakaba and Neher, 2001; Wadel et al., 2007; Wölfel et al., 2007). In RIM1/2 cDKO synapses, the fast release time constant was significantly slower (5.2 ± 1.7 ms, n = 6) than in control synapses (1.8 ± 0.8 ms, n = 5; Figure 5E; p = 0.002), but it was significantly faster than the *slow* release time constant in control synapses, which was 23 ± 3.7 ms (n = 5; Figure 5F; $p < 0.001$). Similarly, when cumulative release traces were arbitrarily fitted with monoexponential functions, the resulting time constant in RIM1/2 cDKO synapses (9.3 ± 1.1 ms; n = 6) was still significantly faster than the slow release time constant in wild-type cells ($p < 0.001$). Both of these comparisons show that the FRP is not simply missing completely but rather that release from the remaining FRP is slowed in the RIM1/2 cDKO synapses.

Figures 5E and 5F show further parameters extracted from the kinetic analysis of transmitter release for each genotype. Overall, the analysis shows a strongly reduced number of readily releasable vesicles in both the FRP and the SRP, as well as a significant, ~2.5-fold slowing of the fast release component.

The kinetics of transmitter release in response to Ca^{2+} influx depends on the intrinsic speed of release, as well as on the "local" $[Ca^{2+}]_i$ that builds up close to the readily releasable vesicles, which, in turn, is a function of the distance between Ca^{2+} channels and vesicles (Neher, 1998; Wadel et al., 2007). The Ca^{2+} uncaging experiments showed that the intrinsic Ca^{2+} sensitivity is reduced in the absence of RIM1/2 (Figure 4). To ask whether the spatial coupling between Ca^{2+} channels and vesicles was impaired as well, we back-calculated the local $[Ca^{2+}]_i$ that was necessary to reproduce the kinetics of the fast release component in response to depolarizations (Figures 5B and 5C, gray traces; Schneggenburger and Neher, 2000). This was done by using the specific sets of kinetic parameters that describe the intracellular Ca^{2+} sensitivities of transmitter release of RIM1/2 cDKO and control synapses (Figure 4). In the examples of Figure 5C, a step-like local $[Ca^{2+}]_i$ signal of 7.7 μM predicted the time-course of the fast release component in the RIM1/2 cDKO synapse, whereas a $[Ca^{2+}]_i$ signal of 9.4 μM was necessary in the case of the control synapse. On average, the back-calculated local $[Ca^{2+}]_i$ signal was 12.0 ± 2.5 μM (n = 5) and 9.0 ± 1.2 μM (n = 6) in control and RIM1/2 cDKO synapses, respectively (Figure 5G; $p < 0.05$). Thus, the local $[Ca^{2+}]_i$ signal experienced by average readily releasable vesicles during a Ca^{2+} current at 0 mV is significantly smaller in RIM1/2 cDKO synapses. This suggests that there are either fewer "local" Ca^{2+} channels around each given readily releasable vesicle and/or that the average distance between Ca^{2+} channels and vesicles is increased in the absence of RIM1/2.

In further experiments designed to analyze a decreased coupling between Ca^{2+} channels and vesicles, we measured the suppression of EPSCs by the slow Ca^{2+} buffer, EGTA-AM (Figure S3). These experiments showed a trend toward a faster block by EGTA-AM in RIM1/2 cDKO synapses, as would be expected for a longer Ca^{2+} channel-vesicle distance (Borst and Sakmann, 1996; Fedchyshyn and Wang, 2005); however, the difference did not reach statistical significance ($p = 0.073$).

RIMs Dock Vesicles to the Active Zone

We showed that RIM1/2 deletion led to a strong reduction of the readily releasable pool (Figures 3–5). Does this reduction of the functional pool size reflect a deficit in priming docked vesicles to fusion competence as suggested before (Koushika et al., 2001; Calakos et al., 2004) or might RIM proteins have an additional role in vesicle docking? To distinguish between these possibilities, we investigated the synaptic ultrastructure of RIM1/2 cDKO calyces and control calyces using serial section transmission electron microscopy (EM) (Figure 6). Large calyx of Held nerve terminals in the MNTB area of both genotypes had overall normal appearance (data not shown). In high-resolution images of active zones, there was a conspicuous reduction in the number of vesicles at active zones and fewer docked vesicles were apparent (Figure 6A), suggesting that RIM1/2 is involved in vesicle docking.

To quantify the spatial distribution of vesicles, we reconstructed entire active zones, taking into account all vesicles within a distance of 300 nm to the active zone membrane (Figure 6B). From the reconstructions, histograms of the shortest membrane-to-membrane distance between each vesicle and the active zone were computed (Figure 6C; n = 18 and 17 active zones for RIM1/2 cDKO and control tissue, sampled over n = 4 calyces each). For the control data, there was a clear peak for the membrane-nearest bin (10 nm or less; Figure 5C, arrow), which most likely represents the pool of docked vesicles (Verhage and Sørensen, 2008). Importantly, in RIM1/2 cDKO synapses, the vesicle number in this membrane-near bin was strongly reduced (Figure 6C; arrow). Figure 6D shows the relative vesicle number (RIM1/2 cDKO/control * 100 for each bin), which illustrates a quite selective decrease in the membrane-near bin, although there was also a modest decrease in the number of vesicles located further away in the cytoplasm (~20%; Figure 5D). Defining docked vesicles as those that are located within 10 nm of the active zone membrane, we found 7.0 ± 4.6 docked vesicles in control synapses (n = 17 active zones) but only 1.5 ± 1.8 in RIM1/2 cDKO synapses (n = 18; Figure 6E; $p < 0.001$). This shows a drastic reduction of the number of vesicles docked at the active zone membrane in RIM1/2 cDKO synapses.

In *C. elegans* synapses, RIM1 enables the lateral localization of docked vesicles close to the presynaptic density (Gracheva et al., 2008). In analogy, it is possible that in mammalian synapses, the loss of RIM proteins could lead to a lateral mislocalization of docked vesicles into areas adjacent to the active zone ("outliers"). To address this possibility, we made flat surface renderings of each 3D-reconstructed active zone and its adjacent plasma membrane (Figure 6F) and then analyzed the density of outlier docked vesicles, which were defined as docked vesicles localized up to 100 nm outside of active zones (Figure 6F, see green symbols). As can be seen in the example images in Figure 6F, active zone size varied greatly between individual contact sites (Schikorski and Stevens, 1997; Taschenberger et al., 2002), but the average active zone size was unchanged between the genotypes (Figures 6G and 6H). Overall, we only found n = 8 and n = 9 outlier vesicles in the set of n = 17 and 18 active zones analyzed here. Normalized to the corresponding membrane area, the density of outliers was similarly low for both genotypes (~3–4 vesicles/μm^2; see Table S1); note that this value is less than 5% of the density of docked vesicles within the active zones of wild-type synapses (Figure 6I). Thus, removal of RIM proteins specifically reduces the density of docked vesicles within the active zone (Figure 5I, $p < 0.001$) but does not affect the number of vesicles docked adjacent to the active zone.

DISCUSSION

We have established a Cre-lox based conditional KO approach at a presynaptically accessible CNS synapse, the calyx of Held. This has allowed us to use presynaptic recordings and Ca^{2+} uncaging, as well as EM analyses of synapses that have developed in vivo, to directly study the presynaptic functions of RIM proteins. We have found three main roles of RIM

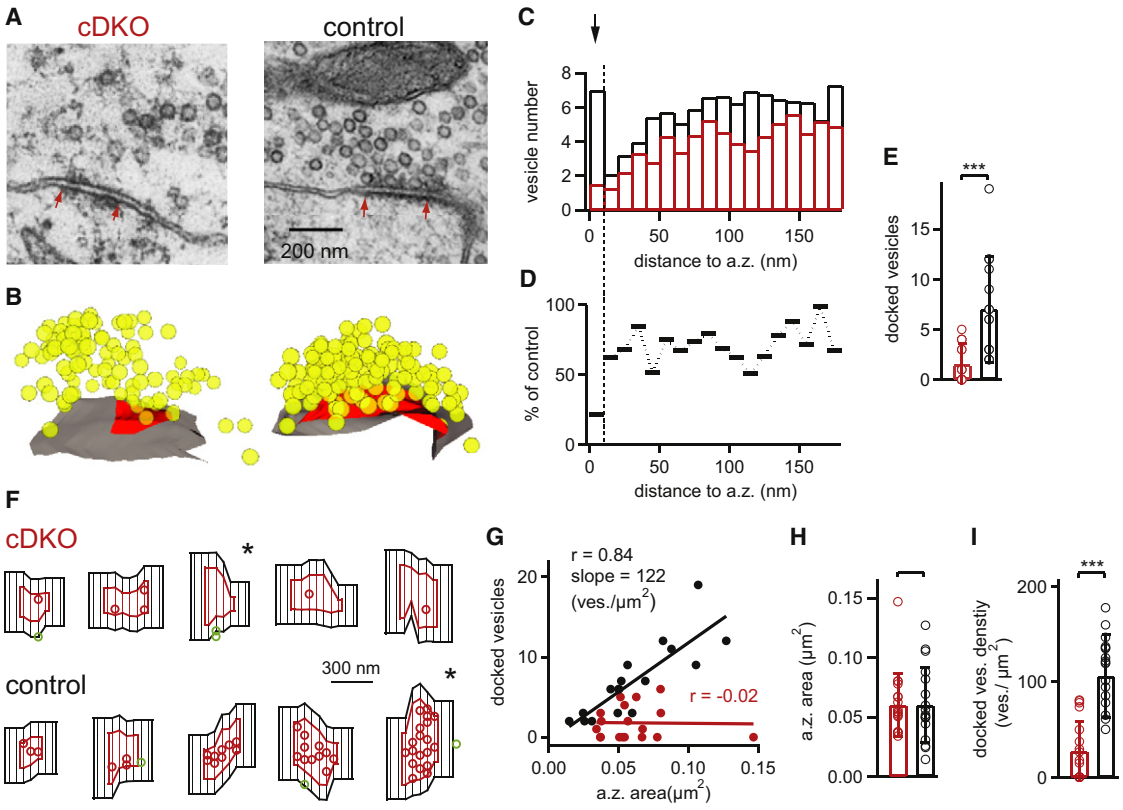

Figure 6. RIM1/2 Docks Vesicles to the Presynaptic Active Zone

(A and B) Representative single EM images of calyceal active zones and 3D reconstructions of the corresponding active zones from a RIM1/2 cDKO mouse (left) and from a control mouse (right) from the same P11 litter. Red arrows in (A) indicate the extent of the postsynaptic density, which was used to measure the active zone sizes. In (B), vesicles are shown in yellow; active zone membrane is indicated in red.

(C) Average histogram of vesicle numbers located at different distances to the active zone; bin width = 10 nm (n = 18 and n = 17 active zones for RIM1/2 cDKO and control mice, respectively). Note that in control synapses, the bin at the shortest distance shows a peak that probably represents the pool of docked vesicles; this peak was strongly reduced in RIM1/2 cDKO synapses (see arrow).

(D) Percentage value of average vesicle numbers shown in (C), calculated as RIM1/2 cDKO values relative to control. Note the much stronger reduction for the membrane-nearest bin (10 nm and less), indicating a strong vesicle docking deficit in RIM1/2 cDKO mice.

(E) Average number of docked vesicles, defined as vesicles located within 10 nm of the active zone membrane. Note the significant decrease in the number of docked vesicles in RIM1/2 cDKO synapses ($p < 0.001$). Also note that because of integer numbers, not all data points are visible (n = 18 and 17 for RIM1/2 cDKO and control, respectively).

(F) Examples of flat surface-rendered active zones (red) and adjacent membrane within 100 nm distance from the active zone (black). Docked vesicles within the active zone and outside are shown as red and green circles, respectively. Five examples for RIM1/2 cDKO (upper) and for control active zones are shown, ordered according to increasing active zone surface. Note the strongly reduced density of docked vesicles in RIM1/2 cDKO synapses, and the only small number of outlier vesicles adjacent to the active zone in both genotypes. The star symbols mark the example active zones shown in (A and B).

(G) Plot of the number of docked vesicles versus active zone area. Linear regression showed a good correlation and near-linear relationship for the control data set with the indicated regression coefficient and slope. In the RIM1/2 cDKO, the data was dominated by a low number of docked vesicles irrespective of active zone size.

(H and I) Average and individual values of active zone area (H), and docked vesicle density per μm^2 of active zone membrane (I). The latter values were obtained by normalizing the docked vesicle numbers (E) to the corresponding active zone area (H).

The error bars represent SD. See also Table S1.

proteins. First, the presynaptic Ca^{2+} current density was strongly reduced about 2-fold in RIM1/2 cDKO nerve terminals. This, together with the parallel study by Kaeser et al. (2011), establishes an important role for RIM proteins in localizing Ca^{2+} channels to the active zone. Second, in agreement with previous studies, we find a reduced pool of readily releasable vesicles (Calakos et al., 2004) and a decreased number of membrane-near vesicles at the active zone, revealing a vesicle-docking function of RIM proteins. Third, RIM proteins speed the rate of transmitter release by increasing the intrinsic Ca^{2+}-sensitivity of release, as well as by contributing to the tight colocalization of readily releasable vesicles with Ca^{2+} channels. Taken together, our study shows that RIM proteins coordinately regulate Ca^{2+} channel targeting, vesicle docking and priming, and Ca^{2+} channel-vesicle colocalization at the presynaptic active zone.

Conditional KO Approach at the Calyx of Held

For the generation of calyx-specific conditional KO mice, we have made use of recently generated floxed mouse lines for RIM1αβ (Kaeser et al., 2008) and RIM2αβγ (Kaeser et al., 2011) and of a previously available Cre knockin mouse line in the Krox20 locus (Voiculescu et al., 2000). The presynaptic neuron pool that generates the large calyx of Held nerve terminals onto MNTB neurons is located in the contralateral ventral cochlear nucleus (VCN) and is largely represented by globular bushy cells (Cant and Benson, 2003). Krox20 is a transcription factor that is highly specifically active in rombomeres 3 and 5 of the developing hindbrain (Voiculescu et al., 2000), which give rise to a majority of neurons in the VCN (Farago et al., 2006; Maricich et al., 2009). We found homogeneous phenotypes among the recorded calyx of Held synapses, which indicates, together with morphological analysis (Figure 1B; L. Xiao, N. Michalski, and R.S., unpublished observations; Renier et al., 2010), that the entire population of calyx of Held-generating neurons stems from Krox20Cre-positive neurons. Thus, the Krox20Cre mouse line enables the conditional removal of floxed alleles at the calyx of Held synapse, which will make it a useful tool to advance our understanding also of other proteins of the presynaptic vesicle cycle.

RIM Proteins Localize Ca^{2+} Channels to the Active Zone

Using direct presynaptic recordings at the nerve terminal, we demonstrated that RIM proteins are essential for localizing Ca^{2+} channels to the active zone, as shown by the clear decrease in the presynaptic Ca^{2+} current density in RIM1/2 cDKO calyces. These direct recordings at the nerve terminal show that RIMs determine presynaptic Ca^{2+} channel density without changing major biophysical parameters of Ca^{2+} channel gating, although we cannot exclude that RIMs influence Ca^{2+} channel inactivation with prolonged pulses (>50 ms, Figure 2; Kiyonaka et al., 2007); this, however, will be relevant only for prolonged presynaptic AP trains. Analyzing RIM-dependent presynaptic Ca^{2+} channel targeting has been limited because previously no KO mice deleting all RIM1/2 isoforms were available (Schoch et al., 2002; Calakos et al., 2004) and because previously investigated synapses, including the *C. elegans* neuromuscular synapse (Koushika et al., 2001), did not allow for measurements of presynaptic Ca^{2+} currents. Using cultured RIM1/2 cDKO neurons, Kaeser et al. (2011) have observed an ~2-fold reduction in Ca^{2+} transients in presynaptic boutons during an AP. This, together with our finding that presynaptic APs are unchanged (Figure 2), is evidence for a reduced Ca^{2+} channel density also at small bouton-like synapses.

What might be the molecular mechanism by which RIM proteins hold Ca^{2+} channels at the active zone? Kaeser et al. (2011) showed that the RIM1 and RIM2 PDZ domains directly bind to the C-terminal sequences of the P/Q- and N-type Ca^{2+} channel α subunits and that the PDZ domain was required to rescue the decreased Ca^{2+} transients and the abnormal Ca^{2+} channel localization. In addition, the proline-rich domain of RIM1/2 was also necessary for the rescue, suggesting that a tripartite interaction between RIM1/2, RIM-BPs (which bind to the proline-rich domain of RIMs; Hibino et al., 2002) and the Ca^{2+} channel α subunits is critical for holding Ca^{2+} channel at the active zone. This, together with the present work, identifies RIM1/2 as a presynaptic scaffolding proteins with a clear role in maintaining a high Ca^{2+} channel density at the presynaptic active zone. Previous work has suggested a role for Bruchpilot, a *Drosophila* gene related to ELKS/CAST proteins, in maintaining presynaptic Ca^{2+} channel density and structural entirety at *Drosophila* presynaptic active zones (Kittel et al., 2006).

Conditional removal of RIM1/2 did not significantly change the relative contribution of P/Q-type and N-type channels to the total presynaptic Ca^{2+} current, despite a strongly reduced total Ca^{2+} current. This finding is different to the situation in P/Q-type (α1A subunit) KO mice (Jun et al., 1999), in which a strong compensatory upregulation of presynaptic N-type channels was observed at the calyx of Held (Inchauspe et al., 2004; Ishikawa et al., 2005). Thus, in the absence of RIM1/2, N-type Ca^{2+} channels are not capable of compensating for the missing P/Q-type channels; therefore, the absence of RIM1/2 probably affects both Ca^{2+} channel α subunits equally.

RIMs' Function in Vesicle Docking and Formation of the Readily Releasable Pool

The calyx synapse has been an ideal preparation to functionally define a fast and a slow subpool of the readily releasable pool (Sakaba and Neher, 2001; Wölfel et al., 2007; Wadel et al., 2007; see Neher, 2006 for a review). Here, we find that conditional removal of all major RIM isoforms leads to a strong, ~70% decrease of the readily releasable pool size as defined by various types of pool-depleting Ca^{2+} stimuli (Figures 3–5). Importantly, we found a very similar decrease of the number of docked vesicles at the active zone (by ~70%; Figure 6), demonstrating a genetic manipulation that leads to a parallel decrease in the number of docked vesicles and of the readily releasable pool size determined functionally. Thus, at the calyx of Held, the amount of vesicle docking seems to determine the size of the readily releasable pool. This conclusion is further supported by the reasonable quantitative agreement between the number of docked vesicles on the one hand (~seven docked vesicle per active zone * 500 ≈3500; assuming that a calyx has ~500 active zones; Sätzler et al., 2002; Taschenberger et al., 2002), and the sum of FRP and SRP vesicles on the other hand (~3000–3500; see Figure 5). This indicates that most docked vesicles belong to the readily releasable pool at the wild-type calyx of Held. Genetic removal of all RIM1/2 isoforms strongly reduced docking and thereby determined the size of the readily releasable pool. This conclusion does not rule out the possibility that an additional priming step is necessary to make docked vesicles fusion competent (see Südhof, 2004 for review) and that RIMs might have an additional role in vesicle priming (Koushika et al., 2001; Calakos et al., 2004).

Further work is needed to unravel the molecular mechanisms by which RIM determines vesicle docking and how vesicle docking and priming are related to each other. The long isoforms of RIMs interact via their N termini with Munc13 and with the small GTPase Rab3 (Wang et al., 1997; Dulubova et al., 2005) and related Rabs including Rab8A, -10, and -26 (Fukuda, 2003). It is thought that the interaction of RIMs with Munc13 is important for priming docked vesicles to fusion competence (Betz et al., 2001) since Munc13 was described as a priming factor with no

role in vesicle docking (Augustin et al., 1999). However, recent studies on Munc13 also suggested a role in docking (Siksou et al., 2009), somewhat blurring the distinction between vesicle docking and priming. Single Rab3A KO mice exhibit a deficit in the activity-dependent recruitment of docked vesicles in synaptosomes (Leenders et al., 2001) and show a vesicle-docking phenotype at the neuromuscular junction (Coleman et al., 2007). Surprisingly, however, quadruple Rab3A/B/C/D KO mice do not exhibit a docking phenotype in cultured hippocampal neurons (Schlüter et al., 2004). Taken together, the interaction of the long RIM isoforms with Rab3 and related Rabs could explain the docking function of RIM proteins, and it is possible that in RIM1α KO mice (Schoch et al., 2002) the docking deficit was compensated for by the continued presence of RIM1β, 2α, and 2β. Thus, our experiments in the context of previous data show that RIM proteins have an important role in vesicle docking.

RIMs Influence Release Probability and the Intrinsic Ca^{2+}-Dependent Speed of Release

A third role of RIM proteins regards the release probability of any given readily releasable vesicle. Kinetic analysis showed a clear slowing of the release of the remaining FRP vesicles in RIM1/2 cDKO synapses (Figure 5). This was mediated, in part, by a reduction of the intracellular Ca^{2+} sensitivity of release demonstrated in Ca^{2+} uncaging experiments (Figure 4), mediated by a so far unknown molecular mechanism of RIM. In addition, there was a defect in the coupling between Ca^{2+} channels and vesicles for FRP vesicles, visible as a decreased local $[Ca^{2+}]_i$ signal that we back-calculated during stimulation of release with presynaptic depolarizations (Figure 5). Thus, RIM proteins contribute to a tight Ca^{2+} channel-vesicle colocalization, a function that probably reflects the interaction of RIMs with Ca^{2+} channels on the one hand and with vesicle proteins like Rab3 on the other hand.

Taken together, establishing a conditional KO approach at a presynaptically accessible CNS synapse has allowed us to dissect multiple intertwined roles of the presynaptic scaffolding protein RIM1/2. Overall, the interaction of RIM proteins with a large number of presynaptic proteins (Schoch et al., 2002) allow RIMs to influence several important functions vital for fast transmitter release: (1) the targeting of Ca^{2+} channels to the active zone, probably mediated by interactions of the central RIM1/2 PDZ domain with Ca^{2+} channel α subunits (Kaeser et al., 2011); (2) vesicle docking and the formation of a standing readily releasable pool important for maintaining fast release during repeated stimuli (Sorensen, 2004); and (3) intrinsic speeding of release and a tighter coupling between vesicles and Ca^{2+} channels. Thus, RIM proteins coordinate multiple functions late in the vesicle cycle that all guarantee a fast speed of Ca^{2+}-evoked release at CNS synapses.

EXPERIMENTAL PROCEDURES

Conditional RIM1/2 KO Mice Specific for the Auditory Brainstem

We identified the Krox20Cre mouse line (Voiculescu et al., 2000; a gift of Dr. Patrick Charnay, Paris, France) as a suitable Cre mouse line that drives Cre expression in calyx of Held-generating neurons of the VCN (Figure 1A and Figure S1). We crossed heterozygous Krox20+/Cre mice with a mouse line that carried a floxed RIM1 allele (Kaeser et al., 2008) as well as a floxed RIM2 allele (Kaeser et al., 2011) (see also Supplemental Experimental Procedures). The offspring of the final breeding pairs gave rise to an expected 50% Cre-positive, RIM1lox/Δ, RIM2lox/Δ mice. Because of germline recombination in the Krox20Cre line (Voiculescu et al., 2000), one of each floxed RIM allele was deleted in these mice (as indicated by the Δ symbol) as confirmed by PCR-based genotyping. Synapses recorded in these mice are referred to as RIM1/2 cDKO synapses (for conditional double KO). Since Cre-expression turns on at ~E9 in Krox20+/Cre mice (Voiculescu et al., 2000), the floxed RIM1/2 alleles should be deleted even before synapses initially form at ~E17 in brainstem. As control mice, we used Cre-negative littermate mice with otherwise the same genetic background; thus, the control mice were heterozygous with respect to the RIM alleles. Cre-positive, RIM1lox/Δ, RIM2lox/Δ mice were viable and fertile and were used for further interbreeding. For the analysis of neuron populations in which Cre-recombinase was active, we crossed Krox20+/Cre mice with tdRFP reporter mice (Luche et al., 2007) and performed anti-RFP and anti-Syt2 immunohistochemistry (see Supplemental Experimental Procedures) to reveal Cre-positive neurons and nerve terminals (Figures 1A and 1B and Figure S1).

Slice Preparation and Electrophysiology

Transverse brainstem slices were prepared from postnatal days 9–11 (P9–P11) mice according to standard methods with a LEICA VT1000S slicer. Paired pre- and postsynaptic whole-cell recordings at the calyx of Held synapse were made with an EPC10/double patch-clamp amplifier (HEKA) under visualization in an upright microscope (Zeiss Axioskop 2 FS) equipped with gradient contrast infrared visualization (Luigs and Neumann) and a 60× objective. Details on the electrophysiological methods and on the composition of the patch pipette and extracellular solutions are provided in Supplemental Experimental Procedures.

EPSC Deconvolution and Data Analysis

Deconvolution of EPSCs to calculate the rates of transmitter release was done as first described by Neher and Sakaba (2001), with routines written in IgorPro. The deconvolution analysis assumes that mEPSC with a double-exponential decay (Schneggenburger and Neher, 2000) add linearly to give rise to an evoked EPSC. The calculated release rates were corrected for a contribution of a spillover glutamate current as described (Neher and Sakaba, 2001). Cumulative release traces were obtained by simple integration of the transmitter release traces without further correction for an assumed recovery process. Cumulative release traces were fitted with the following functions: single-exponential, exponential plus line, double-exponential, double-exponential plus line, and triple-exponential (Wölfel et al., 2007). The best-fit function was selected based on the Bayesian information criterion (BIC; Kochubey et al., 2009). Data are reported as average ± standard deviation (SD) values unless otherwise noted. Statistical significance was evaluated with Student's t test, and accepted at $p < 0.05$. For the comparison of release rates, release delays, and fast release time constants between two data sets at various $[Ca^{2+}]_i$ (Figures 4E–4H), the data sets were double-logarithmized and then assessed for statistical significance by analysis of covariance (ANCOVA). The Ca^{2+}-uncaging data were fitted by a five-site model of Ca^{2+} binding and vesicle fusion (Schneggenburger and Neher, 2000). The following parameters were used for control/RIM1/2 cDKO synapses respectively: k_{on}, $1.65 * 10^8$ / $1.05 * 10^8$ [$M^{-1}s^{-1}$]; k_{off}, 7000/5000 [s^{-1}]; pool size, 1390/315 vesicles. The remaining parameters were the same for both data sets (cooperativity factor *b*, 0.35; final fusion rate γ, 7000 s^{-1}).

Presynaptic Ca^{2+} Uncaging

Ca^{2+} uncaging was done with a DP-10 flash-lamp (Rapp Optoelektronik) according to standard procedures described before (Schneggenburger and Neher, 2000; Wölfel et al., 2007); details are given in Supplemental Experimental Procedures.

Electron Microscopy

Transmission EM was performed in the MNTB area of a RIM1/2 cDKO mouse and its control Cre-negative littermate (both at P11) with standard fixation and resin embedding procedures (see Supplemental Experimental Procedures). Serial images were taken with a Philips CM10 TEM operated at 80 kV at

a magnification of 16,000 times with 10–20 adjacent sections of 50 nm thickness. Only active zones that were completely contained in the series were analyzed. The image series were aligned and active zones, including vesicles and surrounding plasma membrane, were reconstructed in 3D with the Fiji software (http://pacific.mpi-cbg.de/wiki/index.php/Main_Page). The shortest distance from the vesicle membrane to the active zone membrane was then calculated in the 3D model, and all vesicles at distances of less than 300 nm were taken into account. Flat rendering of the active zone surface was done by a MatLab function.

SUPPLEMENTAL INFORMATION

Supplemental Information includes Supplemental Experimental Procedures, three figures, and one table and can be found with this article online at doi:10.1016/j.neuron.2010.12.014.

ACKNOWLEDGMENTS

We thank Heather Murray for expert technical assistance; Dr. Graham Knott (Center for Interdisciplinary Electron Microscopy; EPFL) for help and advice with EM; Dr. Daniel Keller for help with flat surface rendering of active zone profiles; Dr. Patrick Charnay and Dr. Hans Jörg Fehling for the gift of mouse lines; and Dr. Olexiy Kochubey, Dr. Erwin Neher, and Dr. Davide Perkel for comments on the manuscript. This research was supported by grants from the Swiss National Science Foundation (SNF; 31003A_122496) and the Synapsis foundation (both to R.S.).

Accepted: November 22, 2010
Published: January 26, 2011

REFERENCES

Augustin, I., Rosenmund, C., Südhof, T.C., and Brose, N. (1999). Munc13-1 is essential for fusion competence of glutamatergic synaptic vesicles. Nature *400*, 457–461.

Betz, A., Thakur, P., Junge, H.J., Ashery, U., Rhee, J.S., Scheuss, V., Rosenmund, C., Rettig, J., and Brose, N. (2001). Functional interaction of the active zone proteins Munc13-1 and RIM1 in synaptic vesicle priming. Neuron *30*, 183–196.

Borst, J.G., and Sakmann, B. (1996). Calcium influx and transmitter release in a fast CNS synapse. Nature *383*, 431–434.

Bucurenciu, I., Kulik, A., Schwaller, B., Frotscher, M., and Jonas, P. (2008). Nanodomain coupling between Ca^{2+} channels and Ca^{2+} sensors promotes fast and efficient transmitter release at a cortical GABAergic synapse. Neuron *57*, 536–545.

Calakos, N., Schoch, S., Südhof, T.C., and Malenka, R.C. (2004). Multiple roles for the active zone protein RIM1α in late stages of neurotransmitter release. Neuron *42*, 889–896.

Cant, N.B., and Benson, C.G. (2003). Parallel auditory pathways: Projection patterns of the different neuronal populations in the dorsal and ventral cochlear nuclei. Brain Res. Bull. *60*, 457–474.

Castillo, P.E., Schoch, S., Schmitz, F., Südhof, T.C., and Malenka, R.C. (2002). RIM1α is required for presynaptic long-term potentiation. Nature *415*, 327–330.

Chen, Y.A., and Scheller, R.H. (2001). SNARE-mediated membrane fusion. Nat. Rev. Mol. Cell Biol. *2*, 98–106.

Coleman, W.L., Bill, C.A., and Bykhovskaia, M. (2007). Rab3a deletion reduces vesicle docking and transmitter release at the mouse diaphragm synapse. Neuroscience *148*, 1–6.

Coppola, T., Magnin-Luthi, S., Perret-Menoud, V., Gattesco, S., Schiavo, G., and Regazzi, R. (2001). Direct interaction of the Rab3 effector RIM with Ca^{2+} channels, SNAP-25, and synaptotagmin. J. Biol. Chem. *276*, 32756–32762.

Dulubova, I., Lou, X., Lu, J., Huryeva, I., Alam, A., Schneggenburger, R., Südhof, T.C., and Rizo, J. (2005). A Munc13/RIM/Rab3 tripartite complex: From priming to plasticity? EMBO J. *24*, 2839–2850.

Farago, A.F., Awatramani, R.B., and Dymecki, S.M. (2006). Assembly of the brainstem cochlear nuclear complex is revealed by intersectional and subtractive genetic fate maps. Neuron *50*, 205–218.

Fedchyshyn, M.J., and Wang, L.-Y. (2005). Developmental transformation of the release modality at the calyx of Held synapse. J. Neurosci. *25*, 4131–4140.

Fukuda, M. (2003). Distinct Rab binding specificity of Rim1, Rim2, rabphilin, and Noc2. Identification of a critical determinant of Rab3A/Rab27A recognition by Rim2. J. Biol. Chem. *278*, 15373–15380.

Gracheva, E.O., Hadwiger, G., Nonet, M.L., and Richmond, J.E. (2008). Direct interactions between *C. elegans* RAB-3 and Rim provide a mechanism to target vesicles to the presynaptic density. Neurosci. Lett. *444*, 137–142.

Hibino, H., Pironkova, R., Onwumere, O., Vologodskaia, M., Hudspeth, A.J., and Lesage, F. (2002). RIM binding proteins (RBPs) couple Rab3-interacting molecules (RIMs) to voltage-gated $Ca^{(2+)}$ channels. Neuron *34*, 411–423.

Inchauspe, C.G., Martini, F.J., Forsythe, I.D., and Uchitel, O.D. (2004). Functional compensation of P/Q by N-type channels blocks short-term plasticity at the calyx of held presynaptic terminal. J. Neurosci. *24*, 10379–10383.

Ishikawa, T., Kaneko, M., Shin, H.-S., and Takahashi, T. (2005). Presynaptic N-type and P/Q-type Ca^{2+} channels mediating synaptic transmission at the calyx of Held of mice. J. Physiol. *568*, 199–209.

Iwasaki, S., and Takahashi, T. (2001). Developmental regulation of transmitter release at the calyx of Held in rat auditory brainstem. J. Physiol. *534*, 861–871.

Iwasaki, S., Momiyama, A., Uchitel, O.D., and Takahashi, T. (2000). Developmental changes in calcium channel types mediating central synaptic transmission. J. Neurosci. *20*, 59–65.

Jahn, R., Lang, T., and Südhof, T.C. (2003). Membrane fusion. Cell *112*, 519–533.

Jun, K., Piedras-Rentería, E.S., Smith, S.M., Wheeler, D.B., Lee, S.B., Lee, T.G., Chin, H., Adams, M.E., Scheller, R.H., Tsien, R.W., and Shin, H.S. (1999). Ablation of P/Q-type $Ca^{(2+)}$ channel currents, altered synaptic transmission, and progressive ataxia in mice lacking the $\alpha_{(1A)}$-subunit. Proc. Natl. Acad. Sci. USA *96*, 15245–15250.

Kaeser, P.S., Kwon, H.B., Chiu, C.Q., Deng, L., Castillo, P.E., and Südhof, T.C. (2008). RIM1α and RIM1β are synthesized from distinct promoters of the RIM1 gene to mediate differential but overlapping synaptic functions. J. Neurosci. *28*, 13435–13447.

Kaeser, P.S., Deng, L., Wang, Y., Dulubova, I., Liu, X., Rizo, J., and Südhof, T.C. (2011). RIM Proteins Tether Ca2+ Channels to Presynaptic Active Zones via a Direct PDZ-Domain Interaction. Cell *144*, this issue, 282–295.

Kittel, R.J., Wichmann, C., Rasse, T.M., Fouquet, W., Schmidt, M., Schmid, A., Wagh, D.A., Pawlu, C., Kellner, R.R., Willig, K.I., et al. (2006). Bruchpilot promotes active zone assembly, Ca^{2+} channel clustering, and vesicle release. Science *312*, 1051–1054.

Kiyonaka, S., Wakamori, M., Miki, T., Uriu, Y., Nonaka, M., Bito, H., Beedle, A.M., Mori, E., Hara, Y., De Waard, M., et al. (2007). RIM1 confers sustained activity and neurotransmitter vesicle anchoring to presynaptic Ca^{2+} channels. Nat. Neurosci. *10*, 691–701.

Kochubey, O., Han, Y., and Schneggenburger, R. (2009). Developmental regulation of the intracellular Ca^{2+} sensitivity of vesicle fusion and Ca^{2+}-secretion coupling at the rat calyx of Held. J. Physiol. *587*, 3009–3023.

Koushika, S.P., Richmond, J.E., Hadwiger, G., Weimer, R.M., Jorgensen, E.M., and Nonet, M.L. (2001). A post-docking role for active zone protein Rim. Nat. Neurosci. *4*, 997–1005.

Leenders, A.G.M., Lopes da Silva, F.H., Ghijsen, W.E.J.M., and Verhage, M. (2001). Rab3a is involved in transport of synaptic vesicles to the active zone in mouse brain nerve terminals. Mol. Biol. Cell *12*, 3095–3102.

Llinás, R., Sugimori, M., and Silver, R.B. (1995). The concept of calcium concentration microdomains in synaptic transmission. Neuropharmacology *34*, 1443–1451.

Luche, H., Weber, O., Nageswara Rao, T., Blum, C., and Fehling, H.J. (2007). Faithful activation of an extra-bright red fluorescent protein in "knock-in" Cre-reporter mice ideally suited for lineage tracing studies. Eur. J. Immunol. *37*, 43–53.

Maricich, S.M., Xia, A., Mathes, E.L., Wang, V.Y., Oghalai, J.S., Fritzsch, B., and Zoghbi, H.Y. (2009). Atoh1-lineal neurons are required for hearing and for the survival of neurons in the spiral ganglion and brainstem accessory auditory nuclei. J. Neurosci. *29*, 11123–11133.

Neher, E. (1998). Vesicle pools and Ca^{2+} microdomains: New tools for understanding their roles in neurotransmitter release. Neuron *20*, 389–399.

Neher, E. (2006). A comparison between exocytic control mechanisms in adrenal chromaffin cells and a glutamatergic synapse. Pflügers Arch. *453*, 261–268.

Neher, E., and Sakaba, T. (2001). Combining deconvolution and noise analysis for the estimation of transmitter release rates at the calyx of held. J. Neurosci. *21*, 444–461.

Renier, N., Schonewille, M., Giraudet, F., Badura, A., Tessier-Lavigne, M., Avan, P., De Zeeuw, C.I., and Chédotal, A. (2010). Genetic dissection of the function of hindbrain axonal commissures. PLoS Biol. *8*, e1000325.

Sabatini, B.L., and Regehr, W.G. (1996). Timing of neurotransmission at fast synapses in the mammalian brain. Nature *384*, 170–172.

Sakaba, T., and Neher, E. (2001). Calmodulin mediates rapid recruitment of fast-releasing synaptic vesicles at a calyx-type synapse. Neuron *32*, 1119–1131.

Sätzler, K., Söhl, L.F., Bollmann, J.H., Borst, J.G.G., Frotscher, M., Sakmann, B., and Lübke, J.H. (2002). Three-dimensional reconstruction of a calyx of Held and its postsynaptic principal neuron in the medial nucleus of the trapezoid body. J. Neurosci. *22*, 10567–10579.

Schikorski, T., and Stevens, C.F. (1997). Quantitative ultrastructural analysis of hippocampal excitatory synapses. J. Neurosci. *17*, 5858–5867.

Schlüter, O.M., Schmitz, F., Jahn, R., Rosenmund, C., and Südhof, T.C. (2004). A complete genetic analysis of neuronal Rab3 function. J. Neurosci. *24*, 6629–6637.

Schneggenburger, R., and Forsythe, I.D. (2006). The calyx of Held. Cell Tissue Res. *326*, 311–337.

Schneggenburger, R., and Neher, E. (2000). Intracellular calcium dependence of transmitter release rates at a fast central synapse. Nature *406*, 889–893.

Schneggenburger, R., Meyer, A.C., and Neher, E. (1999). Released fraction and total size of a pool of immediately available transmitter quanta at a calyx synapse. Neuron *23*, 399–409.

Schoch, S., and Gundelfinger, E.D. (2006). Molecular organization of the presynaptic active zone. Cell Tissue Res. *326*, 379–391.

Schoch, S., Castillo, P.E., Jo, T., Mukherjee, K., Geppert, M., Wang, Y., Schmitz, F., Malenka, R.C., and Südhof, T.C. (2002). RIM1α forms a protein scaffold for regulating neurotransmitter release at the active zone. Nature *415*, 321–326.

Schoch, S., Mittelstaedt, T., Kaeser, P.S., Padgett, D., Feldmann, N., Chevaleyre, V., Castillo, P.E., Hammer, R.E., Han, W., Schmitz, F., et al. (2006). Redundant functions of RIM1α and RIM2α in $Ca(^{2+})$-triggered neurotransmitter release. EMBO J. *25*, 5852–5863.

Siksou, L., Varoqueaux, F., Pascual, O., Triller, A., Brose, N., and Marty, S. (2009). A common molecular basis for membrane docking and functional priming of synaptic vesicles. Eur. J. Neurosci. *30*, 49–56.

Sorensen, J.B. (2004). Formation, stabilization and fusion of the readily releasable pool of secretory vesicles. Eur. J. Phys. *448*, 347–362.

Südhof, T.C. (2004). The synaptic vesicle cycle. Annu. Rev. Neurosci. *27*, 509–547.

Taschenberger, H., Leão, R.M., Rowland, K.C., Spirou, G.A., and von Gersdorff, H. (2002). Optimizing synaptic architecture and efficiency for high-frequency transmission. Neuron *36*, 1127–1143.

Verhage, M., and Sørensen, J.B. (2008). Vesicle docking in regulated exocytosis. Traffic *9*, 1414–1424.

Voiculescu, O., Charnay, P., and Schneider-Maunoury, S. (2000). Expression pattern of a Krox-20/Cre knock-in allele in the developing hindbrain, bones, and peripheral nervous system. Genesis *26*, 123–126.

Wadel, K., Neher, E., and Sakaba, T. (2007). The coupling between synaptic vesicles and Ca^{2+} channels determines fast neurotransmitter release. Neuron *53*, 563–575.

Wang, Y., and Südhof, T.C. (2003). Genomic definition of RIM proteins: Evolutionary amplification of a family of synaptic regulatory proteins(small star, filled). Genomics *81*, 126–137.

Wang, Y., Okamoto, M., Schmitz, F., Hofmann, K., and Südhof, T.C. (1997). Rim is a putative Rab3 effector in regulating synaptic-vesicle fusion. Nature *388*, 593–598.

Wang, Y., Sugita, S., and Südhof, T.C. (2000). The RIM/NIM family of neuronal C_2 domain proteins. Interactions with Rab3 and a new class of Src homology 3 domain proteins. J. Biol. Chem. *275*, 20033–20044.

Wölfel, M., Lou, X., and Schneggenburger, R. (2007). A mechanism intrinsic to the vesicle fusion machinery determines fast and slow transmitter release at a large CNS synapse. J. Neurosci. *27*, 3198–3210.

Wu, L.G., Westenbroek, R.E., Borst, J.G.G., Catterall, W.A., and Sakmann, B. (1999). Calcium channel types with distinct presynaptic localization couple differentially to transmitter release in single calyx-type synapses. J. Neurosci. *19*, 726–736.

Zenisek, D., Davila, V., Wan, L., and Almers, W. (2003). Imaging calcium entry sites and ribbon structures in two presynaptic cells. J. Neurosci. *23*, 2538–2548.